

Effects of Magnetohydrodynamics on Vortex Shedding past a Confined Square Cylinder

Shailendra Rana ^a, Rajendra Shrestha ^b, Hari Bahadur Dura ^c

^{a, b, c} Department of Mechanical Engineering, Pulchowk Campus, Institute of Engineering, TU, Nepal

Corresponding Email: ^a ranashailendra74@gmail.com, ^b rsfluid@gmail.com, ^c duraharis@gmail.com

Abstract

Two dimensional laminar viscous steady flow of an electrically conducting fluid past a square cylinder placed in magnetic field have been studied. Computational simulations have been performed for Reynolds numbers and Hartmann numbers ranging from 1 to 200 and from 0 to 8 respectively for a fixed blockage ratio $\beta = d/W = 1/8$. The magnetic induction method in magnetohydrodynamics (MHD) module of ANSYS Fluent solver has been employed to compute the flow fields. The effects of transverse magnetic field on vorticity, streamlines and flow coefficients such as drag and lift coefficients have been studied. Results show that the complete suppression of vortex shedding can be achieved and establish a steady flow if a sufficiently strong magnetic field is applied. The average drag coefficient is decreased from 1.3742 to 1.0069 with the increase in Hartmann number from 0 to 3.0 as long as the flow remains unsteady. For flows in the steady regime, the drag coefficient is found to increase with the increment of Hartmann number. Similarly, the amplitude of unsteady lift decreases with the increase in Hartmann number indicating the reduction in strength of shed vortices. A critical value of Hartmann number for Reynolds number of 200 has been found to be 3.6 required for complete suppression of the vortex shedding.

Keywords

MHD, Wake, Vortex Shedding, Hartmann number, Low Magnetic Reynolds Number, Square Cylinder

1. Introduction

The flow over bluff bodies is a classical problem in fluid mechanics which has been extensively studied due to practical engineering applications [1] [2] [3] [4]. Some of the practical engineering applications include heat exchangers, marine risers, road vehicles, pipelines, cooling towers etc. Owing to the practical applications in the real world, there have been massive numerical and experimental studies on the flow around such bodies for over a century. Such bodies may be circular, square, rectangular or triangular in shape. The flow around such bodies, irrespective of their geometry, present many similarities in terms of wake structure at different Reynolds numbers [5]. At very low Reynolds numbers, a creeping flow mechanism is observed where the flow remains attached and takes the shape of the cylinder surface. As the Reynolds number (Re) increases, the flow separates to form a closed steady recirculating region consisting of symmetric twin vortices known as ‘recirculation bubble’ behind the

body. Such flow structure is observed for $Re \leq 40-50$. At higher Reynolds number, the flow becomes unsteady and vortices shed alternately from the top and bottom region of the body leading to the formation of von Karman vortex streets. The unsteady flow exerts fluctuating forces which may cause structural damage to the body due to induced vibrations. The control of such ‘flow-induced vibrations’ is of paramount interest to the researchers. The control of flow-induced vibrations is achievable through the control of vortex shedding which leads to the reduction of unsteady forces acting on the body, thus, significantly reducing unwanted vibrations. In 2016, Rashidi et al provided a comprehensive review of several active and passive control methods implemented for vortex suppression [6]. Some of them are electrical methods, feedback control methods, use of thermal effects, rotary oscillations, etc. Among several control methods, MHD is a new approach of flow control involving the motion of electrically conducting fluids such as liquid metals, electrolytes, plasmas etc. MHD deals with the study

of the motion of electrically conducting fluids under the presence of magnetic field. Whenever an electrically conducting fluid flows under the presence of external magnetic field, it induces an electric current which, in turn, interacts with the magnetic field to produce the Lorentz force. For flows of conducting fluids past bluff bodies, this force act as a damping force which can completely eliminate the periodic vortex shedding and the flow-induced vibrations. Other applications of MHD are pumps, generators, industrial processes in metallurgical industry, material processing in chemical engineering, nuclear engineering etc. For instance, in metallurgical and material processing, the application of magnetic fields includes heating, melting and casting of conducting materials, stirring and levitation of liquid metals.

Many researches regarding the control of flow involving conducting fluids past bluff bodies are already available. In 1974, Bramley investigated the steady two-dimensional incompressible flow of a conducting fluid past a circular cylinder in the presence of streamwise magnetic field using the method of series truncation. It was observed that the flow remains attached to the surface of the cylinder and the flow separation is not seen until the rear stagnation point [7]. In 1985, Kumari & Bansal investigated the slow motion of a viscous, incompressible and electrically conducting fluid around a circular cylinder in the presence of magnetic field parallel to the main flow for two Reynolds numbers i.e. 0.05 and 0.1 using series truncation method. They concluded that the tangential drag coefficient increases with the increase in Stuart number (N) [8]. In 1993, Josserand et al studied the effect of streamwise magnetic field on the flow of a liquid metal past a cylinder. It was observed that the drag could be minimised on the application of magnetic field and von-Karman streets observed behind the cylinder could be eliminated if a sufficiently strong magnetic field is applied [9]. In 2000, Rao & Sekhar investigated the steady two-dimensional incompressible MHD flow past a circular cylinder up to Reynolds number of 500 and $N = 1.3$ in the presence of aligned magnetic field using finite difference method. It was found that as N increases, the suppression of the separation is observed. For small values of N , drag coefficient decreases with the increase of N [10]. In 2007, Singha et al investigated the laminar viscous flow of a conducting fluid past a confined square cylinder for a

fixed blockage ratio $\beta = 1/4$ under the influence of transverse magnetic field at Reynolds number ranging from 50 to 250. It was found that for a steady flow, the separated zone behind the cylinder is reduced as the magnetic field is increased. For flows with periodic vortex shedding and unsteady wake regime, as the magnetic field is increased, the Strouhal number marginally increases. It was also observed that the vortex shedding can be completely suppressed if the sufficiently strong magnetic field is applied. They also suggested a range of minimum Hartmann numbers for different Reynolds numbers at which complete suppression of the vortex shedding could be achieved [11].

In this paper, the effects of magnetohydrodynamics on the laminar incompressible viscous flow of an electrically conducting fluid past a square cylinder for a fixed blockage ratio $\beta = 1/8$ using MHD module of ANSYS Fluent solver are studied. The fluid considered has constant physical properties and are given by: dynamic viscosity $\mu = 1 \text{ kg/ms}$, density $\rho = 100 \text{ kg/m}^3$, electrical conductivity $\sigma = 100 \text{ S/m}$ and magnetic permeability $\mu_0 = 1.257 \times 10^{-6} \text{ H/m}$. The paper investigates the effects of magnetic field on wake structure and flow coefficients.

2. Problem Description and Mathematical Modelling

2.1 Geometrical Configuration

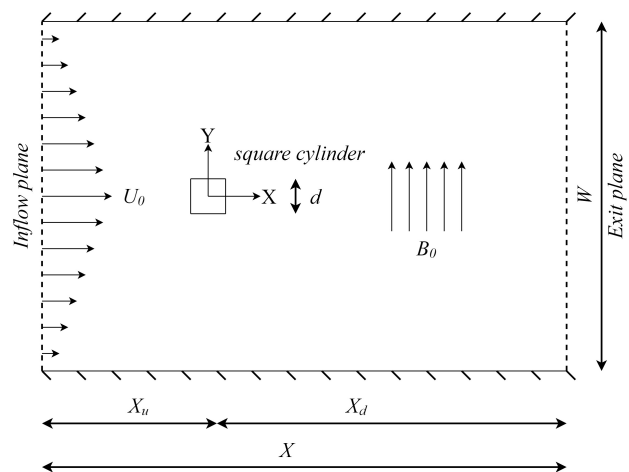


Figure 1: Schematic diagram of the physical model

The problem under consideration is shown in Figure 1. A two-dimensional laminar viscous flow of an electrically conducting incompressible fluid having constant electrical conductivity σ , dynamic viscosity

μ and density ρ around a square cylinder confined in a rectangular channel is considered. The fluid flow with a parabolic inlet velocity U_0 from left to right is considered. A uniform magnetic field B_0 is applied in the transverse direction. The height of the channel is W and d is the side length of the square cylinder. The origin is located at the centre of the cylinder. The non-dimensional total length of the channel is set to $X/d = 50$. The non-dimensional upstream length between the channel inlet to the origin of the cylinder, X_u , is taken as 12.5 whereas the non-dimensional downstream length, X_d , between the origin of the cylinder and the channel outlet is taken as 37.5. The fixed blockage ratio ($\beta = d/W$) is taken as 1/8. All the solids walls are insulated.

Through MHD interactions, an electric field E is induced perpendicular to the plane of the flow, which in turn, gives rise to the secondary magnetic field b parallel to the main flow. The magnetic Reynolds number, $Re_m = \mu_0 \sigma U_0 d$, is in the order of 10^{-5} . Since $Re_m \ll 1$, the strength of induced magnetic field is negligible compared to the applied magnetic field B_0 .

2.2 Governing Equations

A laminar, viscous and incompressible flow of an electrically conducting fluid in the presence of external magnetic field can be described by a set of Navier-Stokes and Maxwell equations. The governing equations are written under three sub-headings as follows:

2.2.1 Navier-Stokes Equations

For incompressible fluids, the continuity equation is defined as:

$$\nabla V = 0 \quad (1)$$

In the presence of external magnetic field, the flow is described by adding proper source term to the momentum equation as follows:

$$\frac{\partial V}{\partial t} + V \cdot \nabla V = -\frac{1}{\rho} \nabla p + \nu \nabla^2 V + \frac{1}{\rho} J \times B \quad (2)$$

Here, the term, $\frac{1}{\rho} J \times B$ in Equation 2 represents the Lorentz force acting in the flow domain.

2.2.2 Maxwell's Equations

A set of Maxwell's equations are stated as follows:

$$\nabla \cdot B = 0 \quad (3)$$

$$\nabla \times E = -\frac{\partial B}{\partial t} \quad (4)$$

$$\nabla \cdot D = q \quad (5)$$

$$\nabla \times H = J + \frac{\partial D}{\partial t} \quad (6)$$

The induction fields H and D are defined as:

$$H = \frac{1}{\mu} B \quad (7)$$

$$D = \epsilon E \quad (8)$$

The magnetic induction method available in MHD module built in ANSYS Fluent has been selected for all simulations.

2.2.3 Magnetic Induction Formulation

The theoretical framework regarding the magnetic induction method is provided by [12] as follows:

According to Ohm's law, the current density can be defined as:

$$J = \sigma E \quad (9)$$

When the fluid is moving defined by velocity field V in the presence of magnetic field B ,

$$J = \sigma(E + V \times B) \quad (10)$$

From Equation 4,

$$\frac{\partial B}{\partial t} = -\nabla \times E \quad (11)$$

From Equation 10,

$$E = \frac{J}{\sigma} - V \times B \quad (12)$$

Taking the curl on both sides in Equation 12,

$$\nabla \times E = \nabla \times \left(\frac{J}{\sigma} - V \times B \right) \quad (13)$$

Inserting Equation 13 into Equation 11, we get,

$$\frac{\partial B}{\partial t} = -\nabla \times \left(\frac{J}{\sigma} - V \times B \right) \quad (14)$$

$$\frac{\partial B}{\partial t} = -\nabla \times \left(\frac{J}{\sigma} \right) + \nabla \times (V \times B) \quad (15)$$

If the displacement current is neglected, we can rewrite Equation 6 as:

$$\nabla \times H = J \quad (16)$$

Using Equation 7,

$$\frac{1}{\mu} (\nabla \times B) = J \quad (17)$$

Substituting Equation 17 into Equation 15, we get,

$$\frac{\partial B}{\partial t} = -\frac{1}{\mu\sigma} \nabla \times (\nabla \times B) + \nabla \times (V \times B) \quad (18)$$

Equation 18 can be rewritten as:

$$\frac{\partial B}{\partial t} = -\frac{1}{\mu\sigma} (\nabla(\nabla \cdot B) - B(\nabla \cdot \nabla)) + V(\nabla \cdot B) - B(\nabla \cdot V) \quad (19)$$

Using Equation 3, we get,

$$\frac{\partial B}{\partial t} = \frac{1}{\mu\sigma} \nabla^2 B + V(\nabla \cdot B) - B(\nabla \cdot V) \quad (20)$$

Equation 20 can be written as:

$$\frac{\partial B}{\partial t} + B(\nabla \cdot V) = \frac{1}{\mu\sigma} \nabla^2 B + V(\nabla \cdot B) \quad (21)$$

Equation 21 represents the magnetic induction formulation derived from Ohm's law and Maxwell's equations. By solving Equation 21, we can obtain B , and using B , we can compute J .

The Reynolds and Hartmann numbers have been defined on the basis of side of the cylinder as: $Re = \frac{\rho U_0 d}{\mu}$ and $Ha = B_0 d \sqrt{\frac{\sigma}{\mu}}$ respectively.

2.3 Grid Structure

Structured non-uniform grids have been generated using ICEM CFD software. Figure 2 shows the expanded view of M4 grid. Four progressively refined grids have been created with constant cell sizes of Δ and δ around the surface of the cylinder and in the adjacent of channel walls respectively. Details of the grids can be found in Table 1.

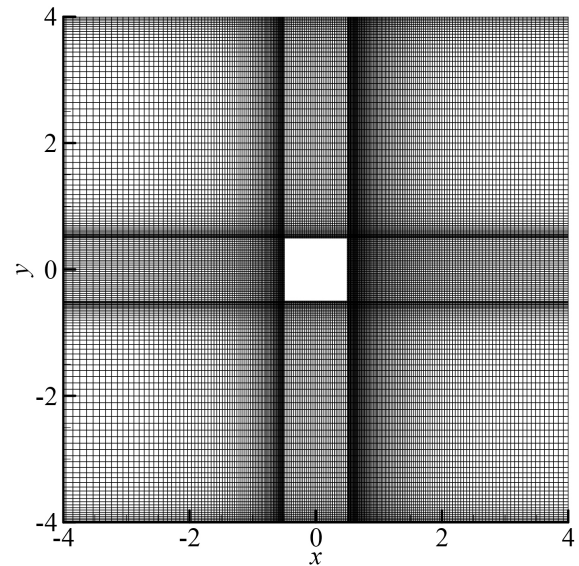


Figure 2: Grid structure

Table 1: Details of the grids

SN	Name of grids	λ	Δ	δ
1	M1	14972	$0.01d$	$0.02d$
2	M2	27022	$0.01d$	$0.02d$
3	M3	42172	$0.01d$	$0.02d$
4	M4	60422	$0.01d$	$0.02d$

2.4 Physics Setup

The SIMPLE algorithm is used for coupling between continuity and momentum equations. For temporal discretization, the second-order implicit scheme has been used. For spatial discretization, the second-order upwind scheme has been used for convective terms while the central difference scheme has been employed for diffusive terms. A convergence criterion of 10^{-7} is found to be sufficient for all the equations [13].

The boundary and initial conditions associated with the physical problem shown in Figure 1 are explained as follows:

a) *At the inflow plane:* At the inlet of the channel, the flow is assumed to be parabolic distribution. The parabolic velocity distribution is used to denote the fully developed laminar flow. In order to assign the parabolic velocity distribution, the following boundary condition has been imposed at the inlet which is given by,

$$u = 1 - \left(\frac{2y}{W}\right)^2, v = 0$$

b) *On the top and bottom walls:* Since the present study considers confined flow across the square cylinder placed in a channel, a *no-slip* boundary condition, that is, $u = 0, v = 0$ has been applied on the top and bottom walls.

c) *On the surface of square cylinder:* *No-slip* condition has been applied on the solid surface of the square cylinder.

d) *At the exit plane:* *Pressure outlet* boundary condition has been applied at the exit plane. Regarding the initial condition, there is no flow inside the channel at the initial time.

2.5 Grid Independence Study

A grid independence study was carried out using four different grids listed in Table 1. Simulations have been performed for $Re = 100$ taking time-step size, $\Delta t = 0.025 s$ for all simulations. It can be observed that the variation in C_d as we move from M1 mesh to M2 mesh is 4.18%. Again, as we move from M2 mesh to M3 mesh, the variation in is less than 1%. As we move further from M3 mesh to M4 mesh, the variation is 0.23%. Similarly, the difference in Strouhal number (St) between M3 and M4 meshes is less than 1%. Figures 3 and 4 shows the variation in the values of C_d and St with the size of the grids.

Hence, for conservative analysis, M4 mesh has been chosen for the rest of simulations.

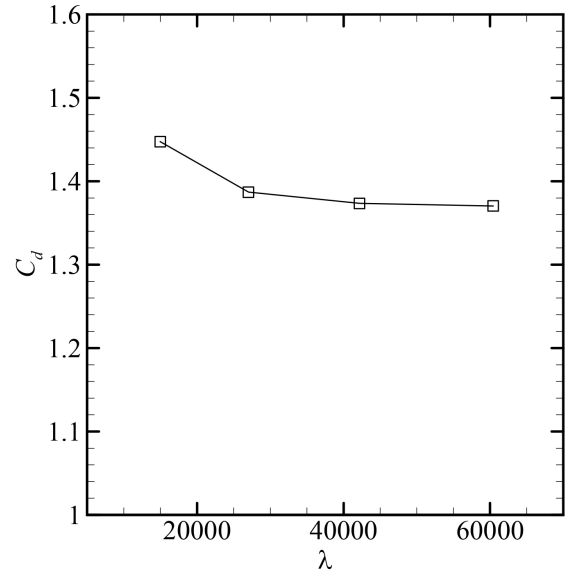


Figure 3: Variation of drag coefficient with number of elements

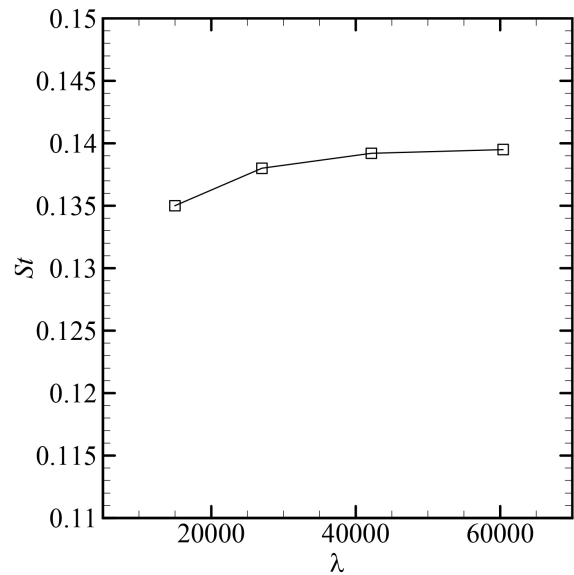


Figure 4: Variation of Strouhal number with number of elements

2.6 Validation

With M4 mesh and boundary conditions, simulations have been performed to compute the values of drag coefficient and Strouhal number for respective Reynolds numbers and compared with the results of Breuer et al[14]. They studied the laminar flow past a confined square cylinder up to $Re = 300$ for a fixed blockage ratio ($\beta = 1/8$) using two different numerical

techniques, namely a lattice-Boltzmann automata and a finite volume method. However, comparison of the present results has only been made against the results obtained from finite volume method. Figures 5 and 6 depict a good agreement between the present results of drag coefficient for $Re = 1-200$ and the published literature. Similarly, the values of Strouhal number for $Re = 75-200$ are also in good agreement with the published literature shown in Figure 7. For instance, the average difference between the present results and the published literature of drag coefficient for $Re = 1-50$ is 1.83 %. Similarly, the average difference between the present results and the published literature of time-averaged drag coefficient and Strouhal number for $Re = 75, 100$ and 200 is 1.15 % and 0.39 % respectively.

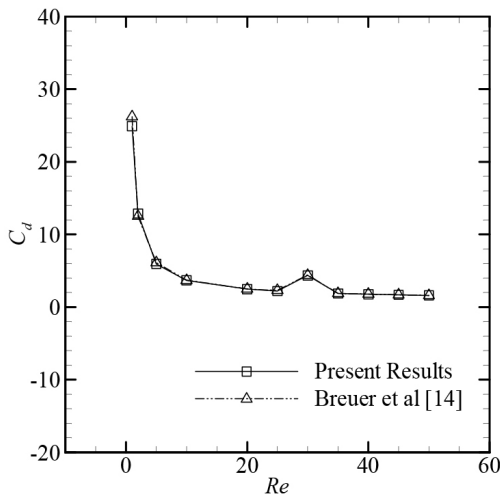


Figure 5: Comparison of drag coefficient against published literature for $Re = 1-50$

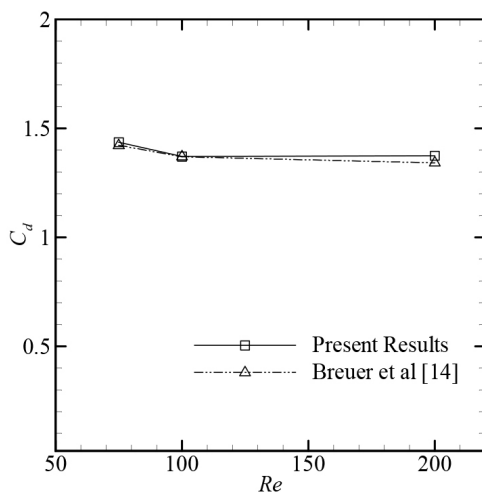


Figure 6: Comparison of drag coefficient against published literature for $Re = 75, 100$ and 200

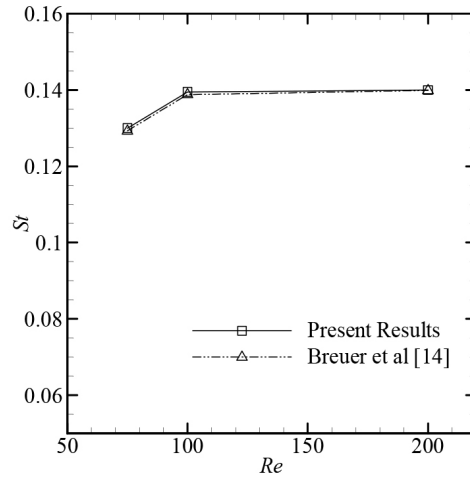


Figure 7: Comparison of Strouhal number against published literature for $Re = 75, 100$ and 200

3. Results and Discussion

3.1 Critical Hartmann number

Critical Hartmann number (Ha_{cr}) refers to the value of Hartmann number at which an unsteady flow converts to a steady flow. In 2007, Singha et al reported a range of minimum Hartmann number for several Re in case of square cylinder under transverse magnetic field [11]. Table 2 presents the required range of minimum Hartmann number for several Re which converts unsteady flow to steady flow.

Table 2: Range of Ha for different Re

SN	Re	Range of minimum Hartmann number
1	150	2.0-3.0
2	200	3.0-4.0
3	250	4.0-5.0

The value of critical Hartmann number has been obtained for $Re = 200$ and compared with the values reported by Singha et al [11] and Turki et al [15]. .

Table 3: Comparison of Ha_{cr} for $Re = 200$ against published literature

SN	Singha et al [11]	Turki et al [15]	Present
1	3.0-4.0	3.662	3.6

The critical Hartmann number (Ha_{cr}) for $Re = 200$ has been found to be 3.6 which is in excellent agreement with the published literature as shown in Table 3. These results indicate good solution

capabilities of magnetic induction method in MHD module built in ANSYS Fluent.

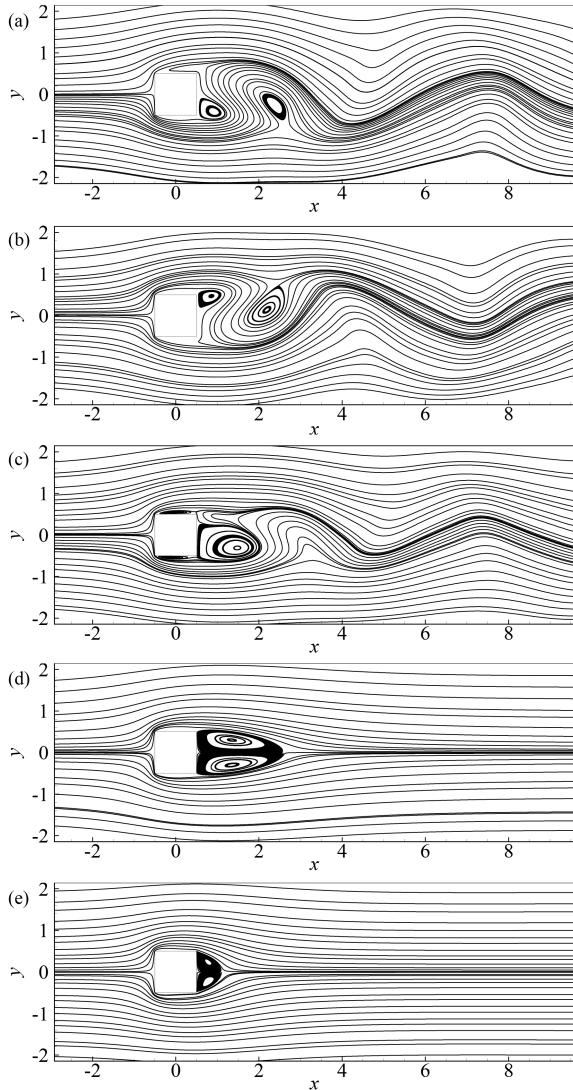


Figure 8: Streamlines at $Re = 200$: (a) $Ha = 0$, (b) $Ha = 1.0$, (c) $Ha = 3.0$, (d) $Ha = 4.0$ and (e) $Ha = 8.0$

3.2 Influence on wake

Figures 8 and 9 depict the contours of streamline and vorticity of the flow at $Re = 200$ under varying magnetic fields in crossflow direction. For $Ha = 0$, the flow at $Re = 200$ is of transient nature evidenced by the presence of alternate shedding of vortices from the top and bottom region of square cylinder as shown in Figure 9 (a). For $Ha < 3.6$, it is observed that the flow still remains in unsteady state depicted by Figures 8 (a)-(c). At $Ha = 3.6$, the vortex shedding phenomena is completely eliminated and the flow assumes steady state, evidenced by the presence of a closed and symmetric recirculating wake as shown in Figure 8

(d). With further increase in Hartmann number, it is observed that the length of the wake is reduced as shown in Figures 8 (d)-(e). The physical explanation behind such phenomena is that the application of transverse magnetic field produces a damping force known as Lorentz force in the upstream direction capable of eliminating the diffusion of vortices. If a sufficiently strong magnetic field is applied, the flow asymmetry and unsteadiness could be completely removed and thus, the flow-induced vibrations could also be completely eliminated.

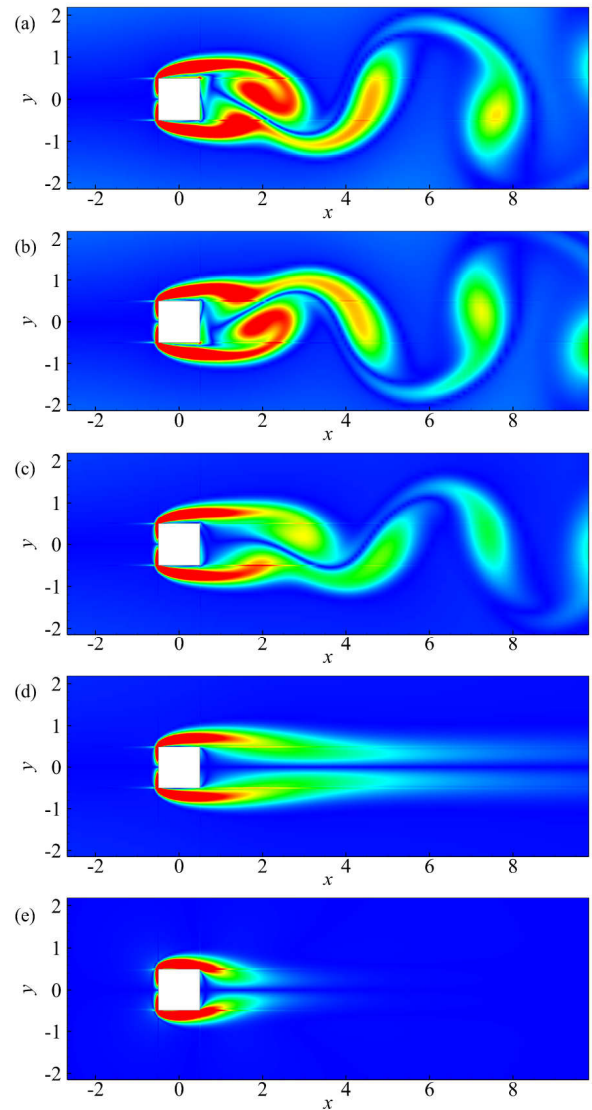


Figure 9: Contours of vorticity at $Re = 200$: (a) $Ha = 0$, (b) $Ha = 1.0$, (c) $Ha = 3.0$, (d) $Ha = 4.0$ and (e) $Ha = 8.0$

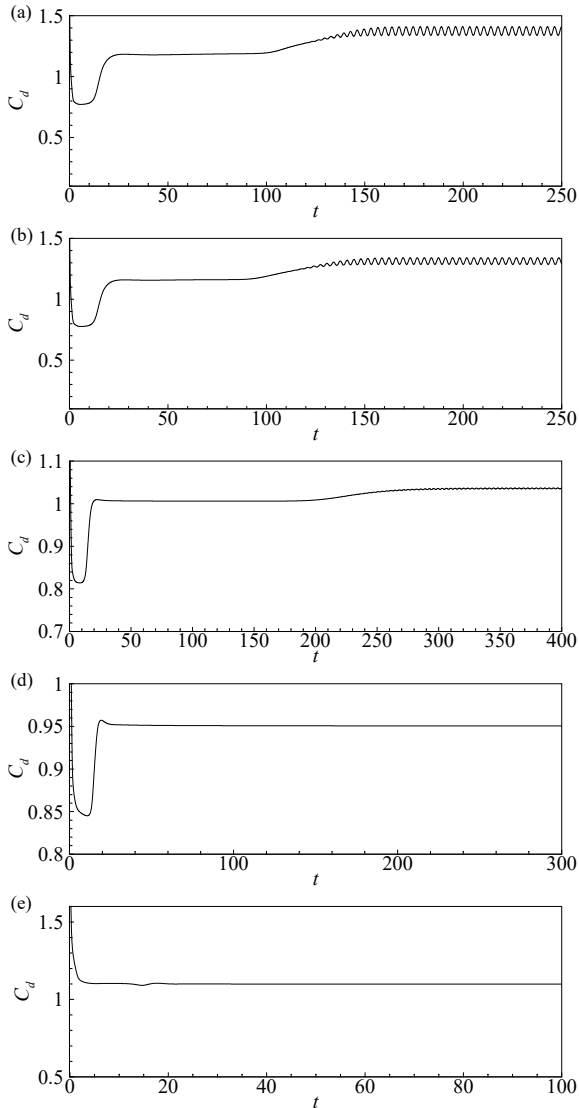


Figure 10: Time history of the drag coefficient with respect to the non-dimensional time (t) at $Re = 200$: (a) $Ha = 0$, (b) $Ha = 1.0$, (c) $Ha = 3.0$, (d) $Ha = 4.0$ and (e) $Ha = 8.0$

3.3 Influence on flow coefficients

Figures 10 (a)-(e) shows the temporal variations of the average drag coefficient at $Re = 200$ for different Hartmann numbers. From Figures 10 (a)–(c), it is seen that the average drag coefficient decreases from 1.3742 to 1.0069 with the increase in Hartmann number from 0 to 3.0 as long as the flow is in unsteady regime. However, when the flow attains steady state on the application of sufficiently strong magnetic field, the drag coefficient is found to increase with further increment of Hartmann number as shown by Figure 10 (d)-(e). The physical explanation can be attributed to the fact that at steady

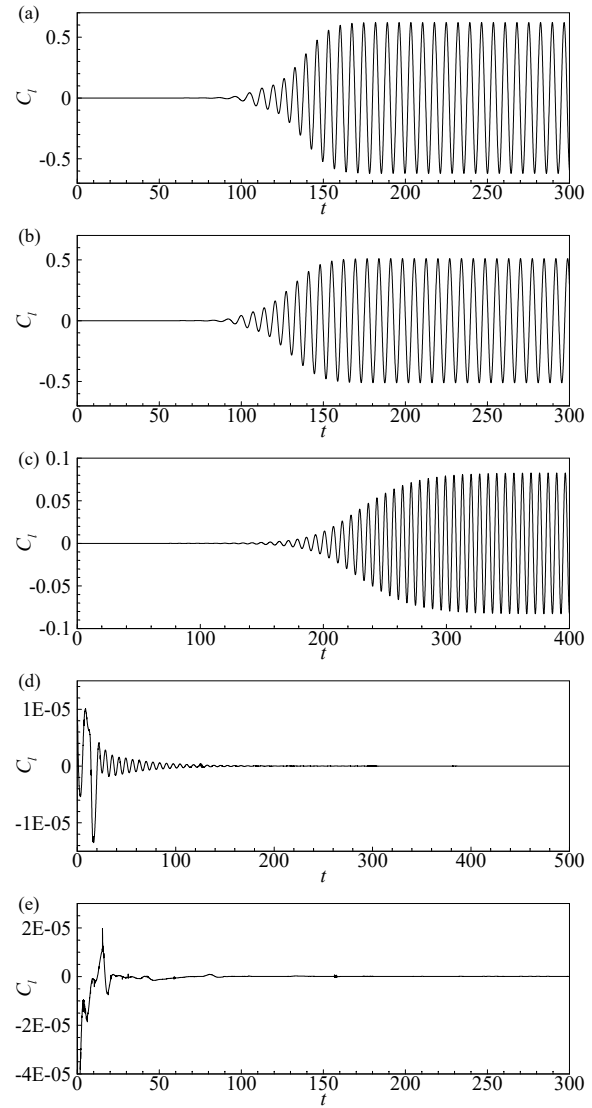


Figure 11: Time history of the lift coefficient with respect to the non-dimensional time (t) at $Re = 200$: (a) $Ha = 0$, (b) $Ha = 1.0$, (c) $Ha = 3.0$, (d) $Ha = 4.0$ and (e) $Ha = 8.0$

state, the fluid flux across any cross-section of the channel is constant causing the pressure drop to increase with the increased amount of Lorentz force to keep on the flow. This increment in pressure drop is due to the pressure increase on the front region of the cylinder, consequently increasing the pressure drag on the body.

The temporal variations of the lift coefficient for $Re = 200$ at different Hartmann numbers are shown in Figure 11 (a)-(e). It is seen that the amplitude of lift coefficient significantly decreases with the increase in Hartmann number from 0 to 8. This implies that the strength of shed vortices has also reduced. After an

initial transient period, it is observed that the average lift coefficient becomes zero which indicates that the flow has attained steady state as shown in Figure 11 (d). With further increase in Hartmann number, it is seen that the time to attain the steady state decreases as shown in Figure 11 (e).

Conclusions

In this paper, a laminar incompressible viscous flow of an electrically conducting fluid past a square cylinder confined in a channel under the presence of transverse magnetic field has been studied. The fluid is assumed to have uniform electrical conductivity. The magnetic Reynolds number is very small so that the induced magnetic field is negligible compared to the applied magnetic field. The magnetic induction method in MHD module built in ANSYS Fluent has been considered to carry out MHD simulations. From the study, the following conclusions are drawn regarding the effects of transverse magnetic field on the flow around square cylinder as follows:

- The complete suppression of vortex shedding is achievable if a sufficiently strong magnetic field is applied.
- The drag coefficient is decreased from 1.3742 to 1.0069 as the Hartmann number is increased from 0 to 3.0 in the periodic laminar regime but starts to increase in the steady flow regime.
- The amplitude of lift coefficient is decreased with the increase in Hartmann number indicating the reduction in strength of shed vortices.
- A critical value of Hartmann number, $Ha_{cr} = 3.6$ has been found for $Re = 200$ at which complete suppression of vortex shedding is observed.

Acknowledgements

The authors are thankful to the technical assistance and support from Department of Mechanical and Aerospace Engineering, Pulchowk Campus by providing access to computer workstations.

Nomenclature

- μ Dynamic viscosity of the fluid medium
- ν Kinematic viscosity of the fluid medium
- ρ Density of the fluid medium

- σ Electrical conductivity of the fluid medium
- d Side length of the square cylinder
- β Blockage ratio
- X_u Upstream length of the computational domain
- X_d Downstream length of the computational domain
- X Total length of the computational domain
- W Height of the computational domain
- H Magnetic field strength
- D Displacement field
- B_0 Applied magnetic field
- B Total magnetic field
- b Secondary magnetic field
- N Stuart number
- Re_m Magnetic Reynolds number
- q Charge
- ϵ Permittivity of the material medium
- μ_0 Permeability of free space
- μ Permeability of material medium
- J Current density
- Ha Hartmann number
- Ha_{cr} Critical Hartmann number
- E Electric field
- C_d Drag coefficient
- C_l Lift coefficient
- St Strouhal number
- Re Reynolds number
- U_0 Maximum parabolic inlet velocity
- V Dimensionless velocity vector
- t Non-dimensional time
- x Streamwise co-ordinate
- y Transverse co-ordinate
- λ Total number of elements
- Δt Time step size
- δ Minimum cell size adjacent to the channel walls
- Δ Minimum cell size around surface of the square cylinder

References

- [1] Arnab Kumar De and Amaresh Dalal. Numerical simulation of unconfined flow past a triangular cylinder. *International journal for numerical methods in fluids*, 52(7):801–821, 2006.
- [2] Amit Dhiman and Radhe Shyam. Unsteady heat transfer from an equilateral triangular cylinder in the unconfined flow regime. *ISRN Mechanical Engineering*, 2011, 2011.
- [3] BN Rajani, A Kandasamy, and Sekhar Majumdar. Numerical simulation of laminar flow past a circular cylinder. *Applied Mathematical Modelling*, 33(3):1228–1247, 2009.
- [4] Pietro Catalano, Meng Wang, Gianluca Iaccarino, and Parviz Moin. Numerical simulation of the flow around a circular cylinder at high reynolds numbers.

- International journal of heat and fluid flow*, 24(4):463–469, 2003.
- [5] Vincent Dousset. *Numerical simulations of MHD flows past obstacles in a duct under externally applied magnetic field*. PhD thesis, Coventry University, 2009.
- [6] Saman Rashidi, Masoud Hayatdavoodi, and Javad Abolfazli Esfahani. Vortex shedding suppression and wake control: A review. *Ocean Engineering*, 126:57–80, 2016.
- [7] JS Bramley. Magnetohydrodynamic flow past a circular cylinder. *Zeitschrift für angewandte Mathematik und Physik ZAMP*, 25(3):409–416, 1974.
- [8] Rama Kumari and JL Bansal. Slow magnetohydrodynamic flow past a circular cylinder. In *Proceedings of the Indian Academy of Sciences-Mathematical Sciences*, volume 94, pages 51–60. Springer, 1985.
- [9] J Jossierand, Ph Marty, and A Alemany. Pressure and drag measurements on a cylinder in a liquid metal flow with an aligned magnetic field. *Fluid dynamics research*, 11(3):107, 1993.
- [10] CV Raghava Rao and TVS Sekhar. Mhd flow past a circular cylinder—a numerical study. *Computational mechanics*, 26(5):430–436, 2000.
- [11] Sintu Singha, KP Sinhamahapatra, and SK Mukherjea. Control of vortex shedding from a bluff body using imposed magnetic field. 2007.
- [12] A Altintas and I Ozkol. Magnetohydrodynamic flow of liquid-metal in circular pipes for externally heated and non-heated cases. 2015.
- [13] Saman Rashidi, M Bovand, JA Esfahani, HF Öztop, and R Masoodi. Control of wake structure behind a square cylinder by magnetohydrodynamics. *Journal of Fluids Engineering*, 137(6), 2015.
- [14] Michael Breuer, J Bernsdorf, T Zeiser, and F Durst. Accurate computations of the laminar flow past a square cylinder based on two different methods: lattice-boltzmann and finite-volume. *International journal of heat and fluid flow*, 21(2):186–196, 2000.
- [15] Hajer Farjallah, Hassan Abbassi, and Saïd Turki. Vortex shedding of electrically conducting fluid flow behind square cylinder under magnetic field. *Engineering Applications of Computational Fluid Mechanics*, 5(3):349–356, 2011.